Atmospheric Environment 316 (2024) 120168

Contents lists available at ScienceDirect

Atmospheric Environment

journal homepage: www.elsevier.com/locate/atmosenv

Assessing the role of atmospheric dispersion vs. emission strength in the southern Po Valley (Italy) using dispersion-normalised multi-time receptor modelling

Federica Crova [a], Alice Corina Forello [a,b], Vera Bernardoni [a], Giulia Calzolai [b,e], Silvia Canepari [c], Stefania Argentini [d], Francesca Costabile [d], Maria Agostina Frezzini [c], Fabio Giardi [b,e], Franco Lucarelli [b,e], Dario Massabò [f,g], Lorenzo Massimi [c], Silvia Nava [b,e], Marco Paglione [h], Giulia Pazzi [b,e], Paolo Prati [f,g], Matteo Rinaldi [h], Mara Russo [h], Sara Valentini [a], Gianluigi Valli [a], Virginia Vernocchi [g], Roberta Vecchi [a,*]

[a] Department of Physics, Università degli Studi di Milano and INFN-Milano, Milan, 20133, Italy
[b] Department of Physics and Astrophysics, Università degli Studi di Firenze, Sesto Fiorentino, 50019, Italy
[c] Department of Environmental Biology, Sapienza Università di Roma, Rome, 00185, Italy
[d] Institute of Atmospheric and Climate Sciences ISAC-CNR, Rome, 00133, Italy
[e] INFN-Firenze, Sesto Fiorentino, 50019, Italy
[f] Department of Physics, Università degli Studi di Genova, Genoa, 16146, Italy
[g] INFN-Genova, Genoa, 16146, Italy
[h] Institute of Atmospheric and Climate Sciences ISAC-CNR, Bologna, 40129, Italy

HIGHLIGHTS

- High PM levels are due to atmospheric stability and emission strength; DN-PMF points out the source emission role.
- Secondary aerosol-dominated factors showed a regional nature.
- Urban aerosol factor was highly enhanced by dispersion-normalisation.

GRAPHICAL ABSTRACT

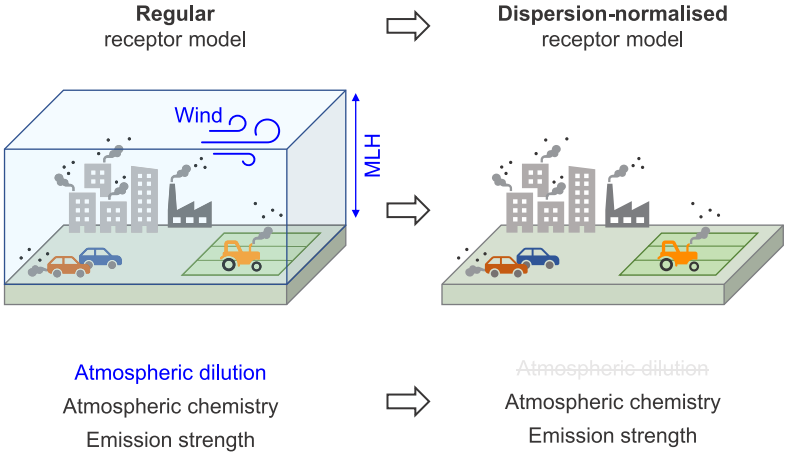

* Corresponding author. Department of Physics, Università degli Studi di Milano, via Celoria 16, 20133, Milan, Italy.
E-mail address: roberta.vecchi@unimi.it (R. Vecchi).

https://doi.org/10.1016/j.atmosenv.2023.120168
Received 18 July 2023; Received in revised form 17 October 2023; Accepted 28 October 2023
Available online 30 October 2023

ARTICLE INFO

Keywords:
Atmospheric stability
Pollution hotspot
Source apportionment
PM_1
Different time resolution
Ventilation coefficient

ABSTRACT

In this paper, we applied the Dispersion Normalised Positive Matrix Factorisation (DN-PMF) approach recently proposed in the literature to provide a more realistic picture of the relative importance of emission strength vs. atmospheric dispersion conditions. The disentanglement of such effects is of great concern in pollution hot spots like the Po Valley (Italy), where particulate matter limit values are exceeded despite the existing abatement measures. To explore the potentiality of the DN-PMF approach – still scarcely applied in the literature – a well-chemically characterised PM_1 (atmospheric particles with aerodynamic diameter <1 μm) dataset comprising samples collected at different time resolutions at an urban background site (Bologna) in the southern Po Valley was used. Indeed, it is well known that shallow mixing layers promote pollutant accumulation but this observation is not enough to exclude an enhancement of emission strength which could be tackled by appropriate abatement strategies.

The source apportionment of sub-micron sized aerosols having a quite long atmospheric residence time in a complex environment like the Po Valley - which is also strongly impacted by secondary aerosol formation on a basin-scale - is generally quite challenging when using receptor models. Due to the availability of a huge dataset with variables having multiple time resolutions, in this work the DN-PMF was implemented in a multi-time resolution approach (MT) to achieve a better source identification and to gain knowledge about the relative importance of atmospheric dilution vs. emissions. A comparison between results obtained by the application of the regular multi time resolution (REG-MT) vs. the DN-MT approach is presented here for the five factors identified (nitrate-dominated, sulphate-dominated, biomass burning, mineral dust, and urban aerosol). The first interesting outcome is that REG-MT and DN-MT results do not point at significant differences in temporal patterns for aerosol components and sources impacting at the basin-scale (i.e. sulphate- and nitrate-dominated aerosol, biomass burning) thus suggesting that the diel modulation of these PM_1 emissions is somehow masked by the stronger variability of the mixing layer. Conversely, contributions from local sources with more pronounced diel variation like traffic are quite well reproduced by DN-MT and the ambient concentrations are enhanced compared to REG-MT. This is an important piece of information highlighting that PM_1 concentrations from local sources have been likely underestimated by REG-MT assessments.

To our knowledge, this is one of the very few applications of DN-MT and the first one at a European site where the huge effort made to implement air pollution containment measures is still not very much effective in reducing PM levels; moreover, in this paper a detailed discussion about the possible interpretation of the output of DN-MT in terms of temporal patterns is reported.

1. Introduction

It is well known that particulate matter (PM) has an impact both at a global scale, e.g., on climate (IPCC, 2021) and at a local scale, especially on human health (Lelieveld et al., 2015; Nozza et al., 2021). The World Health Organisation (WHO) classifies PM among the major health-damaging air pollutants (WHO, 2021) and most of the countries in the world continue to exceed WHO's guidelines for PM exposure (Health Effects Institute, 2020). Nevertheless, at the state of the art, it is still unclear what are the key characteristics and mechanisms primarily responsible for adverse health effects in real-world conditions. This gap of knowledge can be attributed to the extremely complex nature of PM in ambient air in terms of size distributions, physical and chemical properties, the variety of emission sources, formation processes, atmospheric transformations, etc.

To face this lack of information, the PRIN-2017 RHAPS project (Redox-activity and Health-effects of Atmospheric Primary and Secondary aerosol; Costabile et al., 2022) was funded by the Italian Ministry of University and launched with the aim of identifying specific properties of ambient PM_1 responsible for toxicological effects, and linking them to emission sources and atmospheric processes. To reach this goal, extensive field campaigns were carried out in the Po Valley (northern Italy), allowing to achieve a comprehensive physical-chemical PM_1 characterisation obtained through a combination of low- and high-time resolution measurements. The Po Valley is very well known as one of the major polluted areas in Europe (EEA, 2019); indeed, it is the most populated (more than 20 million inhabitants) and industrialised part of Italy, highly impacted by anthropogenic emissions mainly deriving from the transport sector as well as from industrial, agricultural, and livestock farming activities. It is a closed basin shielded from the Alps and Apennines mountains to the north and south, respectively, and its peculiar orography often promotes stagnant atmospheric conditions with shallow mixing layer heights (MLH) and low wind speeds, especially during winter (Crova et al., 2021; Forello et al., 2019; Vecchi et al., 2018, 2019). The combination of intense pollution emissions with poor atmospheric dispersion conditions results in the accumulation of gaseous and particulate pollutants and consequently frequent exceedances of particulate matter concentration limits imposed by European regulations are detected (see e.g., Scotto et al., 2021). Such characteristics make the Po Valley one of the most interesting areas for studying primary and secondary particulate matter complex evolution under real world conditions (see e.g., Larsen et al., 2012; Putaud et al., 2010; Ricciardelli et al., 2017; Vogel and Elbern, 2021). Within this context, this work aims at characterising in detail the emission sources that impacted the investigated site during the RHAPS project field campaigns by performing a source apportionment study where all the information collected is put to the maximum use.

To combine measurements with high- and low-time resolution and to maximise the amount of information gained, the multi-time resolution advanced receptor model was implemented (Ogulei et al., 2005; Zhou et al., 2004) and further developed (Crespi et al., 2016; Forello et al., 2019, 2020; Kuo et al., 2014; Liao et al., 2015; Mooibroek et al., 2022; Sofowote et al., 2018, 2021, 2023; Srivastava et al., 2019) in the Multilinear Engine ME-2 program (Paatero, 1999). By using this approach, each data can be inserted into the model with its native time resolution, and the temporal patterns of the identified emission sources can be reconstructed at a time resolution equal to the shortest sampling interval present in the dataset. In this paper, the multi-time resolution receptor model (in the following referred to as regular multi-time resolution model REG-MT) was used to perform the source apportionment study exploiting variables measured at different time resolutions (1, 2, 24 h), and gaining detailed information about source emission chemical profiles and time patterns at the receptor site.

It is worthy to note that the source apportionment study presented here was quite challenging because the sub-micron sized aerosols have longer residence time in the atmosphere and the atmospheric stability conditions promote secondary aerosol formation and ageing thus enhancing aerosol complexity. Moreover, the field campaigns were

carried out in 2021, when particulate matter concentrations and emission sources behaved a bit differently than usual due to some restrictions related to COVID-19 pandemic still in force.

To separate the effect of atmospheric dispersion from source emission rates (including atmospheric chemistry processes), Dai et al. (2020) have recently proposed the dispersion-normalised Positive Matrix Factorisation (DN-PMF) approach where input data are the measured concentrations of each species normalised by the ventilation coefficient (VC). The latter is given by the product of MLH and mean wind speed and used as an indicator of atmospheric dilution; compared to traditional PMF results, the output gives source emission information with reduced influence of local meteorology. The dispersion-normalisation approach has still been little explored in the literature (Chen et al., 2022a, 2022b; Dai et al., 2021; Gu et al., 2022; Kim et al., 2022; Park et al., 2022) and applied only a few times to a multi-time resolution modelling approach (Sofowote et al., 2021, 2023); in this work, by exploiting the availability of MLH and wind speed data measured at the same site with high time resolution, it was implemented in the multi-time factorisation (DN-MT). To the authors' knowledge, no examples of DN-MT application are available for European sites and it is noteworthy that in this paper we provide a possible interpretation of the temporal patterns related to the actual strength of source emission and atmospheric chemistry processes; this was discussed in much more detail compared to currently published papers. This piece of information can be useful for air quality management as the emission sources can be better identified and tackled taking into account the masking due to atmospheric dilution effects on the observed concentrations.

2. Materials and methods

2.1. Field measurements

Field campaigns were carried out in Bologna (BO), which has about 400 000 inhabitants and is located in the southern Po Valley, at the foot of the Apennines mountain chain. It is mainly impacted by anthropogenic activities related to urban emissions (traffic and residential heating) as well by agricultural and livestock activities which are largely diffused in its surroundings. It is also important to note that around the city there are trafficked highways. The monitoring site (44°31′29″ N, 11°20′27″ E) is located in the National Research Council (CNR) research area, which can be considered representative of the urban background as it is about 2 km from the main railway and about 7 km from the major highway and there are no relevant industrial activities nearby. The measurement campaigns were performed in the periods 21 January 2021–18 March 2021 during winter, and 8 June 2021–14 July 2021 during summer; the starting time for 24-h resolution samples was set at 8 a.m. (Local Time). In the following, time will be always expressed as local time (LT), i.e., UTC+1 during winter and UTC+2 during summer. Online and off-line parallel measurements were carried out in order to get a comprehensive PM_1 physical and chemical characterisation; multiple sampling lines operated in parallel to acquire all the samples needed to reach the goals of the RHAPS project. A detailed description of the site and the operated instrumentation can be found in Costabile et al. (2022); therefore, only the information relevant to the PM_1 dataset exploited in this work is summarised below and minimum detection limits (MDLs) and analytical uncertainties can be found in Table S1.

PM_1 daily mass concentration was retrieved on PTFE filters (Pall R2PJ047, Pall Life Sciences, Ann Arbor, MI, USA) by gravimetric technique using an automatic sample changer and a Sartorius microbalance with a sensitivity of 1 μg. Elemental concentrations (Na, Mg, Al, Si, P, S, Cl, K, Ca, Ti, V, Cr, Mn, Fe, Ni, Cu, Zn, Se, Br, Rb, Sr, Y, Zr, Mo, Ba, and Pb) were determined on these samples by Particle Induced X-Ray Emission (PIXE) analysis at the INFN-LABEC accelerator facility (Lucarelli et al., 2014). On parallel 24-h samples collected on pre-fired quartz-fibre filters (Pallflex Tissuquartz 2500 QAO-UP, Pall Life Sciences, Ann Arbor MI, USA) different punches were analysed by different analytical techniques: major ions (Cl^-, NO_3^-, SO_4^{2-}, Na^+, NH_4^+, K^+, Mg^{++}, Ca^{++}) were determined by Ion Chromatography (IC) analysis (Piazzalunga et al., 2013); levoglucosan (1,6-Anhydro-beta-glucopyranose) by HPLC-PAD (Piazzalunga et al., 2010); elemental and organic carbon fractions (EC and OC) by thermal-optical transmission (TOT) analysis with an offline OCEC Carbon Aerosol Analyser (Sunset Laboratory Inc., Tigard, OR, USA) by applying the NIOSH5040 temperature protocol.

Elemental concentrations with 1-h (winter samples) and 2-h (summer samples, characterised by lower ambient aerosol concentrations) resolution were measured by PIXE (Calzolai et al., 2015). These high-time resolution samples were collected using the STRAS sampler (Size and Time-Resolved Aerosol Sampler), recently developed in-house to replace the streaker sampler (D'Alessandro et al., 2003), which is outdated and no longer on the market. In this work, the STRAS sampler was operated with a PM_1 inlet and the samples were collected on a polycarbonate filter.

EC and OC concentrations were available with 2-h resolution by a Sunset Field Thermal-Optical Analyser (Model-4 Semi-Continuous OC-EC Field Analyzer - Sunset Laboratory Inc., Sunset Laboratory Inc. Tigard, OR, USA).

The non-refractory PM_1 chemical components (sulphate, nitrate, ammonium, chloride, and organic aerosol OA) were measured with 2.5-min time resolution by the High-Resolution Time-of-Flight Aerosol Mass Spectrometer (HR-AMS, Aerodyne Research) (Canagaratna et al., 2007) following the set-up, protocols and data analysis procedures described in Paglione et al. (2020). Data were then averaged on 1-h to reduce data noise and to assure a better comparability and harmonisation with all the other variables.

To gain information on the atmospheric dilution conditions, the mixing layer height (MLH) was computed from turbulence parameters measured at a sampling frequency of 10 Hz by an ultrasonic anemometer uSonic-3 (Metek GmbH, Germany) positioned at a height of 3.3 m above ground level by following the procedure described in Vecchi et al. (2019); wind speed values were also obtained by the same instrument.

To be used as external check (see Sections 3.1 and 3.2), an estimate of PM_1 mass concentrations was also retrieved exploiting particle number size distribution data (details on the methodology can be found in Costabile et al., 2017) measured by the combination of a Mobility Particle Size Spectrometer (TROPOS SMPS) and an aerodynamic particle sizer (APS, TSI).

2.2. Modelling methods

2.2.1. Multi-time resolution receptor model

In the multi-time resolution receptor model firstly reported by Zhou et al. (2004), the basic bilinear equation of PMF is expanded as

$$x_{sj} = \frac{1}{t_{s2} - t_{s1} + 1} \sum_{k=1}^{P} f_{kj} \sum_{i=t_{s1}}^{t_{s2}} g_{ik} \eta_j + e_{sj} \quad (1)$$

to allow a factorisation of input data x_{sj} into the matrices **F** (factor chemical profiles, matrix element f_{kj}) and **G** (factor temporal contributions, matrix element g_{ik}) with different time resolutions without the need of averaging high-time resolution data or interpolating low-time resolution data beforehand. In Equation (1), s, j, and k representthe sample, the species, and the factor, respectively; t_{s1} and t_{s2} indicate the start and the end times for the s^{th} sample, whose temporal length is expressed in terms of discrete time units i, i.e., the shortest sampling interval time in the considered dataset; this means that factors temporal contributions in the **G** matrix have the time resolution of one time-unit. η_j is the adjustment factor for replicated species measured by different samplers and/or analytical methods at a different time resolution.

This main equation is implemented in the Multilinear Engine ME-2 program (Paatero, 1999) and solved by minimising the object function Q, defined as the squared sum of the uncertainty-scaled residuals deriving from Equation (1) and auxiliary equations (Equation S1). In this

work, the auxiliary equations included in the model were a regularisation equation (Equation S2) to smooth time series contributions, a mass balance equation (Equation S3) forcing the sum of concentrations of the species to be equal or smaller than the total PM mass concentration, a normalisation equation for factors in the **G** matrix, and pulling equations, when needed (see Section S1 for further details).

In this work, to evaluate the robustness of the solution the bootstrap analysis (BS, for details see e.g. Norris et al., 2014) implemented in the MT by Crespi et al. (2016) and dQ-controlled perturbation or displacement of factor profile (DISP, for details see e.g. Paatero et al., 2014) analysis implemented in the MT by Mooibroek et al. (2022), were carried out.

2.2.2. Dispersion-normalised multi-time resolution analysis

To better understand the impact of atmospheric dilution in source contribution patterns retrieved by receptor modelling, the dispersion-normalised PMF (DN-PMF) approach (Chen et al., 2022a, 2022b; Dai et al., 2020, 2021; Gu et al., 2022; Kim et al., 2022; Park et al., 2022; Sofowote et al., 2021, 2023) was applied to the MT by normalising the input data by the ventilation coefficient (VC), which quantifies the atmospheric dilution (Tiwari et al., 2016). The VC can be considered as an index of the volume where particulate matter is diluted per unit of time, and for each sampling interval i it is defined as the product of the MLH and the mean wind speed v during the time interval i:

$$VC_i = MLH_i \bullet v_i \tag{2}$$

A single value of VC is computed for each row in the dataset (i.e., for each sampling interval). The normalisation of input data is performed by multiplying each species concentration in sample i for the corresponding VC_i and dividing by $\overline{VC}$, which is the average value of VC over the whole sampling period:

$$x_{ij}^{DN} = x_{ij} \bullet \frac{VC_i}{\overline{VC}} = x_{ij} \bullet VC^* \tag{3}$$

where x_{ij}^{DN} are the DN input data; the term $VC_i/\overline{VC}$ will be referred to as VC*. The same normalisation is applied to data uncertainties used in the multi-time receptor model as data weights. The $\overline{VC}$ was calculated as the average value of 1-h resolution VC data over the winter and summer sampling periods ($\overline{VC} = 215.9\ m^2\ s^{-1}$); thus, concentrations were scaled to the values they would have had if the VC_i were equal to the mean $\overline{VC}$ over the whole sampling period. This means that when VC_i is low (e.g., during the night and/or with shallow mixing layer and/or low wind speeds), the ambient concentrations which are high due to poor dilution are scaled downward, while when VC_i is high (e.g., at noon and/or with high mixing layer and/or high wind speed), the actual concentrations which are low due to the stronger dilution are increased.

The obtained concentration x_{ij}^{DN} and the corresponding uncertainties are then used as input for the DN-MT. As output, the two matrices of factors temporal contribution $\mathbf{G^{DN}}$ (matrix element g_{ik}^{DN}) and chemical profile $\mathbf{F^{DN}}$ (matrix element f_{kj}^{DN}) are obtained. The resulting $\mathbf{F^{DN}}$ values typically exhibit very similar values to the ones obtained in the application of the regular multi-time resolution model (REG-MT) since emission sources remain the same; however, slight differences can be present because some input concentrations x_{ij}^{DN} are drastically decreased when VC* is very low, and the factorisation process is strongly driven by input values approaching zero (Paatero et al., 2005). The $\mathbf{G^{DN}}$ values represent emission source temporal contributions without the influence of atmospheric dilution: therefore, they give important information about the actual emission strength (including atmospheric chemical processing). To keep the $\mathbf{G^{DN}}$ values consistent with input data ambient concentrations and comparable with the REG-MT results, a de-normalisation must be applied to the output values as shown in equation (4):

$$g_{ik}^{deDN} = g_{ik}^{DN} / VC^* \tag{4}$$

where g_{ik}^{deDN} are the matrix elements of the de-normalised matrix $\mathbf{G^{deDN}}$.

BS and DISP analyses were performed also on the DN-MT solutions following the same approaches mentioned in Section 2.2.1.

2.3. Input dataset preparation

In this work 1-h was chosen as the base time unit in the model; indeed, the largest part of our data have such time resolution as it is suitable to describe emission source patterns and atmospheric dilution processes.

Adjustment factors η_j were all set to unity, since a pre-homogenisation step over replicated species measured by different instruments was performed before inserting data into the input matrix **X**. Thus, replicated species concentrations measured at high time resolution (1 and 2-h) were averaged over 24-h and compared with the corresponding daily sample concentrations. Overall, a good agreement was found and the homogenisation factor (HF) was applied only to a few variables (see Table 1). For such cases, concentrations sampled at 24-h were considered the benchmark since their concentrations are usually far from MDL and determined with high accuracy; therefore, HF was used as the multiplying factor applied to high-time resolution species concentrations.

The signal-to-noise ratio (S/N) criterion (Norris et al., 2014) was used to classify variables and weak variables (S/N < 1) were excluded from the analysis with the exception of summertime levoglucosan (S/N = 0.6, see Table S2). Indeed, the latter is a well-known tracer for biomass burning emissions with significant ambient air concentrations in winter (largely ascribed to domestic heating) while, as expected, during the summer its concentrations were close to or lower than MDLs due to the reduced biomass burning impact and its depletion due to photochemical processing (Hennigan et al., 2010). Aiming at detecting possible small contributions from this source, it was included in the input dataset although strongly downweighed by multiplying the associated uncertainties by a factor of 4. The same downweighting was applied to Ca concentrations otherwise it was very spread in all chemical profiles and gave large scaled residuals (not shown).

SO_4^{2-}, NO_3^-, NH_4^+, and OA measured at high time resolution by HR-AMS were inserted in the model with uncertainties reported in Table S1.

A variable selection to avoid double counting for SO_4^{2-}/S, K^+/K, Ca^{2+}/Ca, and OC/OA was also carried out (see Table 1 for details about the final input dataset).

PM_1 mass concentrations were strongly downweighed (4 times their value) (Kim et al., 2003).

The selected variables were pre-treated following Polissar et al. (1998) although for missing values a different approach has been adopted. In previous works (e.g., Forello et al., 2019, 2020; Zhou et al., 2004) missing values were substituted by linear interpolation and then downweighed otherwise artificial peaks in the **G** contributions could be observed. This issue might arise when the time coverage of the high time resolution data is low compared to the one of low time resolution data.

Table 1
Selected species for this study and time resolutions for each season.

Season	Species at 1-h resolution	Species at 2-h resolution	Species at 24-h resolution
Winter	NO_3^-, SO_4^{2-}, NH_4^+, OA, Al, Si, K (HF = 1.5), Ca, Fe, Cu, Zn (HF = 1.9), Pb	EC	PM_1 mass, Levoglucosan, NO_3^-, SO_4^{2-}, NH_4^+, Al, Si, K, Ca, Mn, Fe, Cu, Zn, Pb, EC
Summer	NO_3^-, SO_4^{2-}, NH_4^+, OA	Al, Si, K (HF = 1.7), Ca, Fe, Cu (HF = 1.5), Zn	PM_1 mass, Levoglucosan, NO_3^-, SO_4^{2-}, NH_4^+, Al, Si, K, Ca, Mn, Fe, Cu, Zn, Pb, EC

In the dataset used in this work, only few high-time resolution data were missing (<9% in winter, <12% in summer); therefore, missing data were considered as empty cells in the input matrix and the related equations were not written for them. To check the validity of this approach, a comparison between the two methodologies for treating missing data was also performed obtaining a good agreement (on average differences less than 10% on temporal patterns).

The final input matrix **X** consisted of 3145 samples distributed over 2208 time units; winter and summer datasets were inserted together into the model as data available from different seasons allow a better separation among species with similar seasonal features (for instance nitrate and biomass burning emissions) and therefore lead to more robust

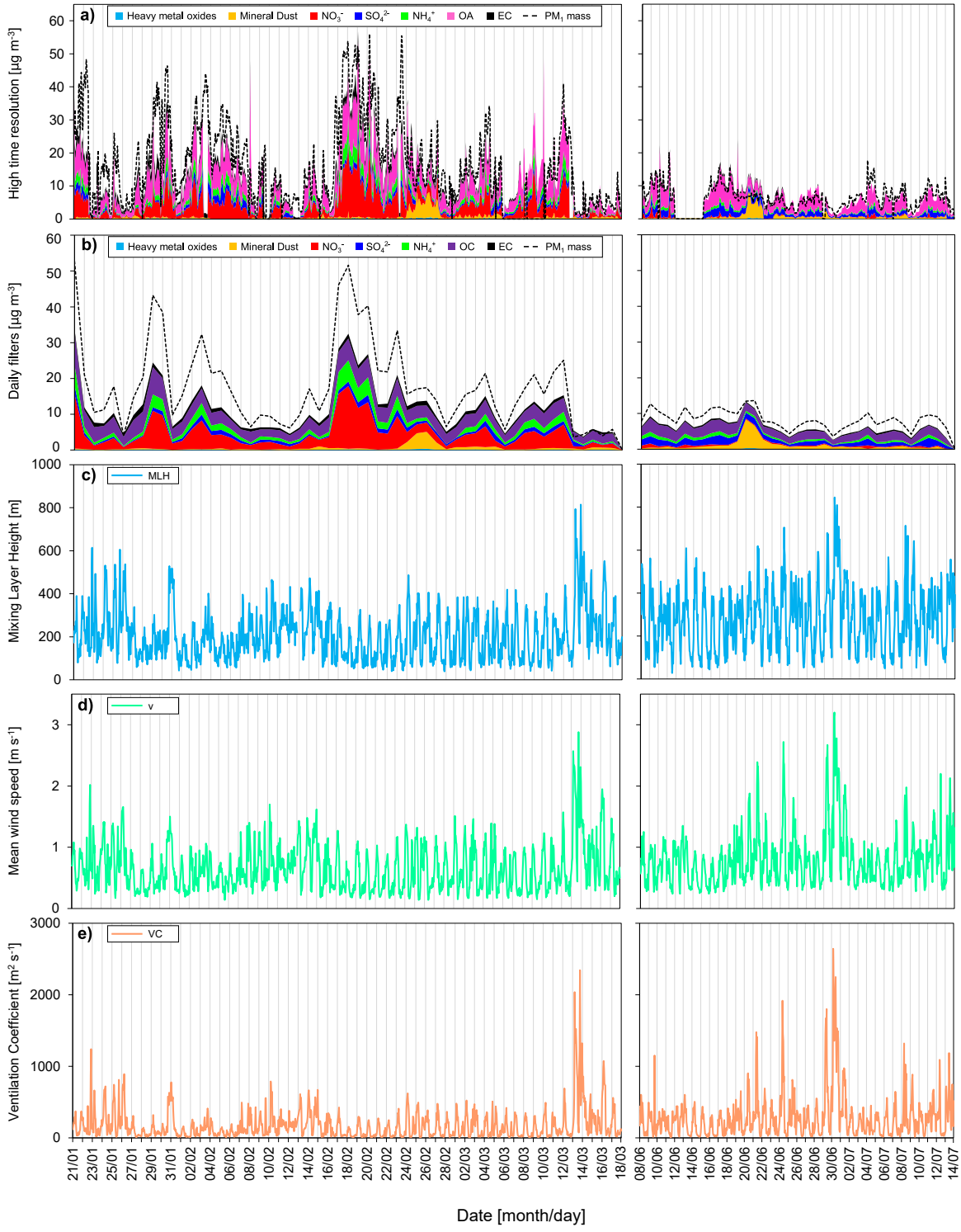

Fig. 1. Overview of PM_1 components and atmospheric parameters related to dilution detected in BO. The left panels refer to winter and right panels to summer. Panels a) and b) show concentrations of major species measured at high time resolution (winter: 1 h resolution, EC at 2 h resolution; summer: 2 h resolution) and on daily filters, respectively. Panels c), d), and e) show mixing layer heights (MLH), mean wind speeds (v), and ventilation coefficient (VC) at hourly resolution. Vertical grey lines indicate 8 a.m. (LT) of each day.

results (Paatero et al., 2005). The error model em = −14 was used for the main equation with c_1 = input uncertainty (obtained as described above), $c_2 = 0$, $c_3 = 0.1$ (Paatero, 2012) (see Section S1 for further details); all the analyses were performed in the robust mode (Brown et al., 2015).

The same methodology was applied to the DN-MT modelling approach, where the input matrix $\mathbf{X^{DN}}$ was the same used in the REG-MT but concentrations and uncertainties were multiplied by VC* (Equation (3)), as explained in Section 2.2.2.

3. Results and discussion

3.1. Overview of measured data

Fig. 1a and b shows species concentrations at high- and low-time resolution, respectively, for the winter and summer campaigns. For high resolution data (Fig. 1a), PM_1 estimated from size distribution data is reported as a proxy for hourly mass concentrations. During winter, BO was strongly impacted by organic aerosol and nitrate accounting on average for about 35% and 19% of PM_1 mass, respectively; in summer the dominant components were organic aerosol (on average 56%) and sulphate (on average 20%).

Episodes of Saharan dust transport occurred during both seasons with peaks in the period 24–27 February and 19–22 June (as confirmed by satellite images reported in Costabile et al., 2022). Interestingly, huge increases in mineral dust concentrations (about 11 and 8 times higher in winter and summer episodes, respectively) were also clearly detected in the sub-micron sized fraction.

A few short-lasting peaks dominated by organic aerosol (see Fig. 1a) were due to an emergency usage of a diesel generator close to the sampling area but they must be considered an exceptional source contribution due to failure in the main energy supply system. PM_1 average mass concentration measured on filters was 18.3 ± 12.1 μg m^{-3} in winter and 8.5 ± 2.5 μg m^{-3} in summer (standard deviations represent the concentration variability). Wintertime average value is considerably lower than what was reported from other works in the Po Valley (Masiol et al., 2014; Squizzato et al., 2013, 2016; Valotto et al., 2014; Vecchi et al., 2004, 2008); this was somehow expected because of the lockdown stringency measures imposed in that period, mainly regarding mobility limitation (night curfews, prohibition on movements between regions and/or municipalities, prohibition on travels to visit private homes and to reach second homes, etc.), and the closure of commercial and leisure activities.

The mass closure on daily filters was retrieved by computing mineral dust and heavy metal oxides following Marcazzan et al. (2004), and by including major inorganic ions (NO_3^-, SO_4^{2-}, NH_4^+), EC, and OC (Figure SF1). The average unaccounted mass was about 30% and 28% for winter and summer, respectively. It is noteworthy that in the mass closure performed replacing OC with OA, the unaccounted mass decreases to 17% and 11% for low- and high-time resolution samples, respectively. It can thus be assumed that approximately half of the unaccounted mass is due to the OC-to-OA conversion factor, and the undetected components (mainly water) contribute slightly less during summer and this behaviour can be related to reduced relative humidity values (average RH was about 71% in winter and 51% in summer).

Fig. 1c, 1d, and 1e display meteorological parameters useful to describe atmospheric dilution, i.e., MLH, mean wind speed, and VC. At the investigated site, median values of MLH maxima ranging from 384 m to 500 m and minima from 63 to 74 m in winter and summer, respectively. Wind speed is often very low, with a median value of 0.56 m s^{-1} in winter and 0.72 m s^{-1} in summer. Therefore, during the monitoring campaigns stable atmospheric conditions typical of the Po Valley were detected very often. Exceptions can be observed during limited periods when stronger winds enhanced the atmospheric dilution (e.g., around 14 March and 30 June) and a drop of PM_1 concentrations was registered; opposite, an accumulation of PM_1 concentration can be seen in correspondence of lower MLH and wind speeds (e.g., 16–23 February). In Fig. 1c the mixing layer showing shallow height during the night and increased thickness during daytime can be observed in both seasons. Mean wind speed values (Fig. 1d) show a similar temporal pattern and the same obviously holds for VC (Fig. 1e).

3.2. Regular multi-time resolution model results

Starting from the application of REG-MT, solutions from 3 to 7 factors were explored; the number of model runs was set at 30, and the base-case solutions corresponding to the minimum Q values (see Section S1) were analysed in detail. The most robust base-case solution was the 5-factors one (minimum $Q = Q_{main} + Q_{aux} = 7511.68$); the factors were assigned to nitrate-dominated, sulphate-dominated, biomass burning, mineral dust, and urban aerosol. The chosen solution was characterised by a good agreement between the values predicted by the model and the measured ones ($R^2 > 0.7$ for all variables but Ca and Pb with and $R^2 = 0.6$). The PM_1 mass concentrations inputted as 24-h values were reconstructed hourly by the MT model; it is noteworthy that these hourly values compare well with the estimates given by particle number size distribution data, used as external check (see Figure SF3). Moreover, when averaging on 24-h the predicted hourly PM_1 values, the agreement with mass concentrations measured on daily samples was very good ($R^2 = 0.89$). The unexplained variation of the F matrix (EVF) was lower than 0.10 for all the variables. Finally, the uncertainty-scaled residuals (Norris et al., 2014) were randomly and symmetrically distributed in the interval [-3,3] (see Figure SF4). BS and DISP analyses were performed; overall, the main tracers and contributors in each profile were characterised by narrow BS and DISP intervals (Figure SF5), thus confirming the solution robustness. In the following, a detailed description of the REG-MT source-to-factor assignment is given.

Two factors associated with secondary aerosol were identified and labelled as nitrate-dominated and sulphate-dominated aerosol. Indeed, in both chemical profiles, organic aerosol was among the most contributing species together with sulphate, nitrate, and ammonium; the presence of organics with secondary species such as ammonium nitrate and ammonium sulphate is very commonly observed in the Po Valley (e.g., Farao et al., 2014; Forello et al., 2019, 2020; Larsen et al., 2012; Masiol et al., 2020; Paglione et al., 2020; Scotto et al., 2021; Tositti et al., 2014; Venturini et al., 2014).

The factor identified as nitrate-dominated aerosol (Fig. 2a) is characterised by very high EVFs for NO_3^- and NH_4^+. NO_3^- is also the main contributor in the profile (59%), followed by OA (22%) and NH_4^+ (18%). These features suggest the presence of ammonium nitrate, i.e., secondary inorganic aerosol typically originated from gaseous precursors. The mass contribution of this factor is the most significant during winter, accounting for about 38% of the PM_1 mass (see Fig. 3a and Table 2); this is very typical of the Po Valley (Forello et al., 2019; Scotto et al., 2021; Vecchi et al., 2018; and therein cited references), which is largely impacted by gaseous pollutants like NO_x and NH_3 emitted by activities such as traffic, residential heating, industrial emissions, agricultural field fertilisation, livestock settlements, etc., and by atmospheric stability. On the opposite, nitrate-dominated factor concentrations drastically drop during summer giving a negligible contribution (about 6%) as the ammonia and nitric acid chemical equilibrium is shifted towards the gaseous phase due to the higher temperatures (Seinfeld and Pandis, 2016). The trace concentrations of potassium in the chemical profile suggest that likely biomass burning emissions are mixed to a small extent with this factor due to the similarity in seasonal temporal patterns, as already observed in the literature (e.g., Forello et al., 2020; Scotto et al., 2021; Venturini et al., 2014).

The factor identified as sulphate-dominated aerosol (Fig. 2b) accounts for the largest EVF value of SO_4^{2-} and quite high EVF are also associated with OA. In the chemical profile, the most significant contribution is given by OA (59%), followed by SO_4^{2-} (28%), NH_4^+ (8%), and EC (8%). The significant concentrations of SO_4^{2-} and NH_4^+ in the

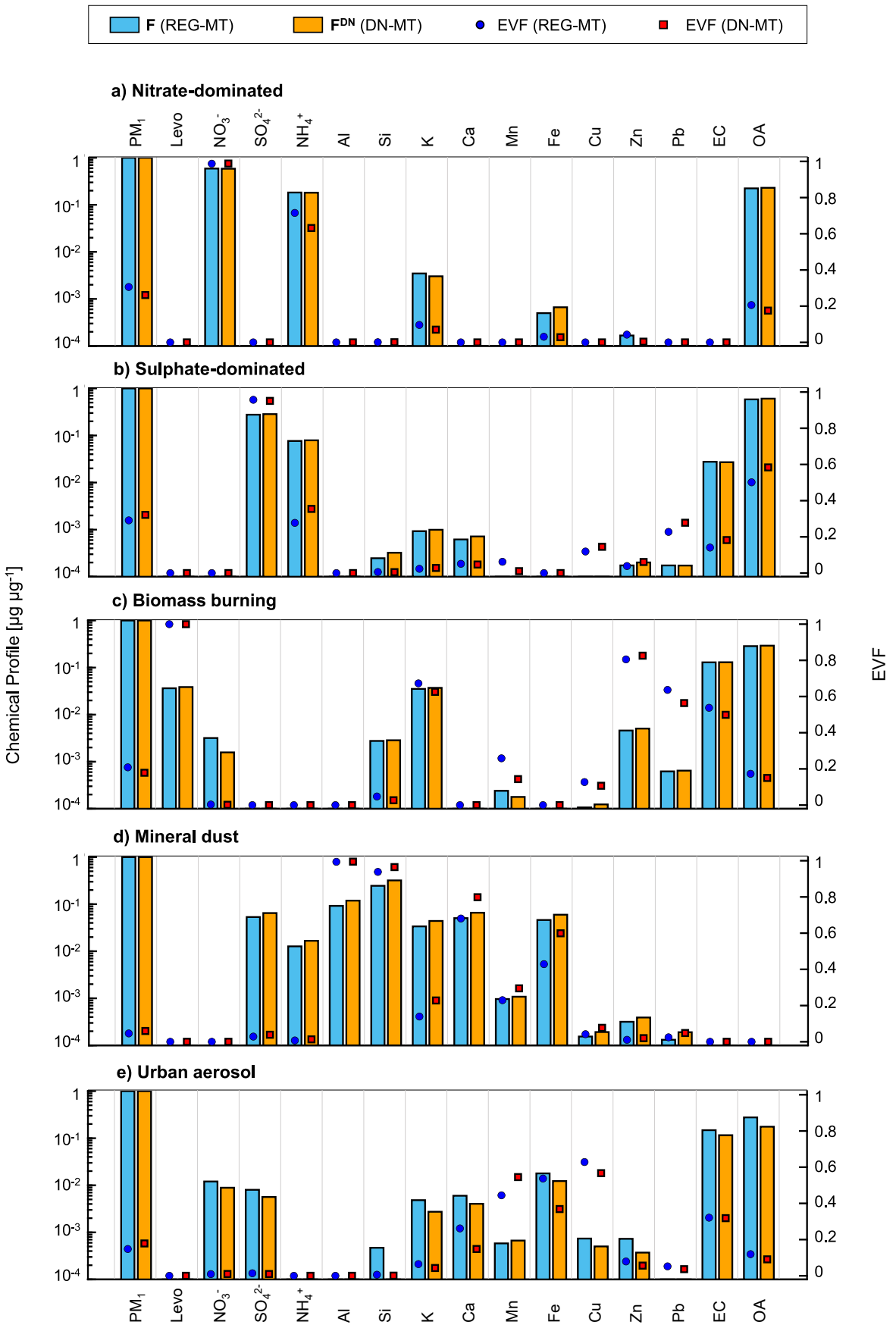

Fig. 2. Factors chemical profiles and EVF values. Vertical bars indicate the chemical profile (**F** and $\mathbf{F}^{DN}$ matrices) normalised by PM_1 mass in each factor (blue, left, solid bars: REG-MT; orange, right, solid bars: DN-MT); dark blue circles and red squares represent EVF for REG-MT and DN-MT, respectively.

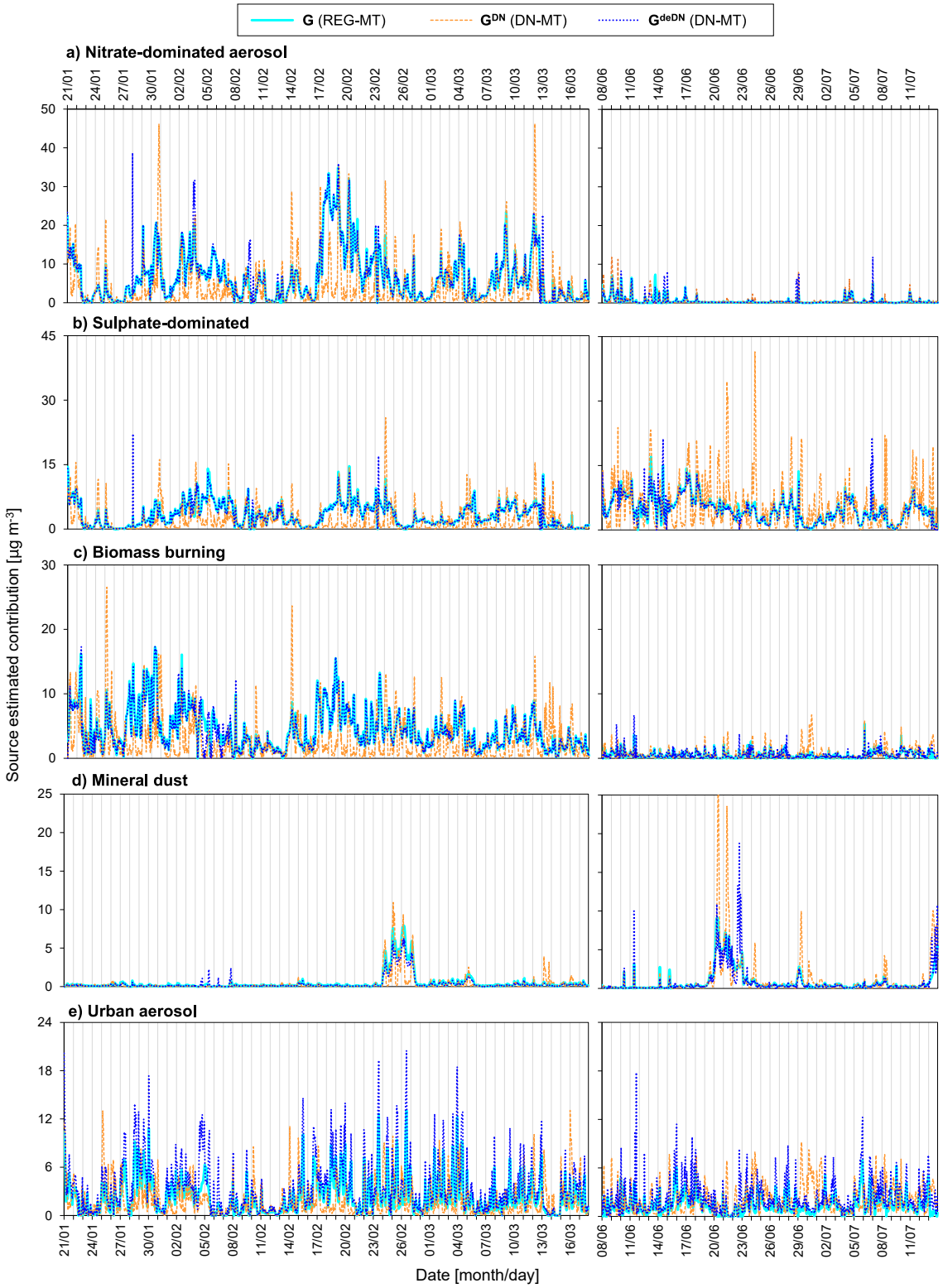

Fig. 3. Factors temporal patterns reconstructed by the model at 1-h resolution, given by **G** (REG: solid, light blue line), $\mathbf{G}^{\mathbf{DN}}$ (DN: dashed, orange line), and $\mathbf{G}^{\mathbf{deDN}}$ (deDN: dotted, dark blue line) matrices. Left and right panels are winter and summer temporal series, respectively. Vertical grey lines indicate 8 a.m. (LT) for each day.

profile suggest the formation of ammonium sulphate from gaseous precursors; due to the very low local SO_2 emissions the presence of ammonium sulphate in the Po Valley is often related to regional aerosol formation (Crosier et al., 2007) or to long-range air masses transport episodes as already observed in the same area as reported by e.g., Vecchi et al. (2009). The average absolute contribution of this source was about 50% higher in summer (Table 2), and its shares in PM_1 were about 19% in winter and 60% in summer indicating the relevance of enhanced photochemical activity during warmer months promoting the formation of sulphates in the atmosphere (Seinfeld and Pandis, 2016). The

Table 2
Average (mean [95% CI]) absolute and percentage source estimated contributions for winter and summer given by different modelling approaches (REG-MT stands for regular multi-time model, and DN-MT is for dispersion normalised multi-time model) and calculated by averaging **G** matrix temporal series (DN-MT results refer to the de-normalised matrix $\mathbf{G}^{\mathbf{deDN}}$). The percentage difference was calculated as (DN-MT – REG-MT)/REG-MT using the mass contribution apportioned by the two approaches. (*) indicates when the differences are statistically significant according to the Mann-Whitney test performed with the R 'stats' package (Bauer, 1972; R Core Team, 2021), p-value<0.01. Slope and R^2 are the parameters of the linear regression (OLS) of DN-MT versus REG-MT temporal patterns.

Factors	Winter	Summer
Nitrate-dominated	REG-MT: 6.50 [6.16,6.84] μg m^{-3} (38%) DN-MT: 6.62 [6.27,6.96] μg m^{-3} (37%) Difference = 2% Slope = 0.98; R^2 = 0.94	REG-MT: 0.50 [0.44,0.57] μg m^{-3} (6%) DN-MT: 0.55 [0.47,0.63] μg m^{-3} (6%) Difference = 9% Slope = 0.97; R^2 = 0.67
Sulphate-dominated	REG-MT: 3.25 [3.11,3.40] μg m^{-3} (19%) DN-MT: 3.19 [3.05,3.33] μg m^{-3} (18%) Difference = −2% Slope = 0.95; R^2 = 0.93	REG-MT: 4.88 [4.69,5.08] μg m^{-3} (60%) DN-MT: 4.76 [4.56,4.96] μg m^{-3} (53%) Difference = −3% Slope = 0.95; R^2 = 0.86
Biomass burning	REG-MT: 4.39 [4.22,4.56] μg m^{-3} (26%) DN-MT: 4.26 [4.09,4.42] μg m^{-3} (24%) Difference = −3% Slope = 0.97; R^2 = 0.95	REG-MT: 0.49 [0.45,0.52] μg m^{-3} (6%) DN-MT: 0.54 [0.50,0.59] μg m^{-3} (6%) Difference = 12% Slope = 1.00; R^2 = 0.65
Mineral dust	REG-MT: 0.48 [0.42,0.54] μg m^{-3} (3%) DN-MT: 0.37 [0.33,0.42] μg m^{-3} (2%) Difference = −23% (*) Slope = 0.75; R^2 = 0.98	REG-MT: 0.84 [0.74,0.93] μg m^{-3} (10%) DN-MT: 0.81 [0.69,0.93] μg m^{-3} (9%) Difference = −3% (*) Slope = 0.95; R^2 = 0.60
Urban	REG-MT: 2.30 [2.18,2.41] μg m^{-3} (14%) DN-MT: 3.36 [3.19,3.52] μg m^{-3} (19%) Difference = 46% (*) Slope = 1.46; R^2 = 0.94	REG-MT: 1.43 [1.36,1.50] μg m^{-3} (18%) DN-MT: 2.28 [2.15,2.40] μg m^{-3} (25%) Difference = 59% (*) Slope = 1.49; R^2 = 0.73

presence of EC and other trace metals suggests, a partial mixing with primary source contributions that can occur for example when sulphate condenses on primary particles previously emitted in the atmosphere; this is in agreement with previous studies at urban sites (see e.g., Amato et al., 2016; Forello et al., 2019).

The factor assigned to biomass burning (Fig. 2c) is characterised by EVF equal to unity for levoglucosan, which is a very well-known tracer for biomass combustion formed by the pyrolysis of cellulose (Li et al., 2021; Vincenti et al., 2022); high EVF values - although with very low mass contributions - are also observed for Zn, K, Pb, and EC. The most contributing species in the chemical profile are OA (29%) and EC (13%), while smaller contributions are given by levoglucosan and K (4% each). As concerns the presence of heavy metals, notably Zn and Pb, in the biomass burning profile is not unusual in the Po Valley (see e.g., Bernardoni et al., 2011; Larsen et al., 2012; Masiol et al., 2020; Scotto et al., 2021) but also reported at different sites (e.g., Amato et al., 2016; Anttila et al., 2008; Hansen et al., 2001; Hovorka et al., 2015; Narodoslawsky and Obernberger, 1996; Ozgen et al., 2017; Tissari et al., 2008; Yao et al., 2023). This factor is the second major contributor to PM_1 (26%, see Table 2) during the coldest months (Fig. 3c) as it is mainly ascribed to the widespread use of biomass fuel for domestic heating (Scotto et al., 2021) while, as expected, in summer its relative contribution is much less (6%). As for the temporal patterns, the higher contribution of biomass burning during nocturnal hours at the same site was related to residential heating by previous literature studies (see e.g., Paglione et al., 2020) and explained as a combination of more intense emissions and lower MLHs during those hours. Interestingly, in this work an additional contribution to PM_1 concentrations was detected during morning hours (see Fig. 4e) likely pointing at the effect of the change in house heating needs due to the widespread smart working activities during the partial lockdown measures.

The factor associated with mineral dust (Fig. 2d) shows the highest EVFs for Al and Si, which are typical crustal elements (Mason, 1966) and the major contributors to PM_1 mass in this source (34%). Also Ca, Fe, and Mn have not negligible EVFs but they account for a 5% share each at maximum. The temporal pattern (Fig. 3d) clearly shows that Saharan dust transport events occurred in both seasons (see Section 3.1) giving the most relevant mass contribution in this factor, with peak concentrations about 18 and 8 times higher (in winter and summer, respectively) than the rest of the campaign, which is more impacted by local soil dust resuspension. The small amount of SO_4^{2-} in the chemical profile can be ascribed to sulphate enrichment of mineral dust, as already reported in the literature (see e.g., Sullivan et al., 2007). The mass apportioned by this factor is the lowest in winter (about 3%, see Table 2; it decreases to about 1% by excluding the transport episode), while during summer the relative contribution becomes larger (about 10%, decreased to about 5% when excluding the Saharan dust transport episode), because in this season drier meteorological conditions promote dust resuspension.

Finally, the factor associated with urban aerosol (Fig. 2e) shows higher EVF values for some heavy metals such as Cu, Fe, Mn, and for EC providing the typical signature of traffic emissions (Thorpe and Harrison, 2008; Viana et al., 2008). OA and EC contribute mostly to the chemical profile (28% and 15%, respectively); other very small contributions are given by Fe (2%), NO_3^-, SO_4^{2-}, and Ca (1% each). As already mentioned, secondary species may derive from their condensation on primary particles, indicating a partial mixing with secondary components. Soil-related elements can be associated with road dust resuspension (Amato et al., 2009; Thorpe and Harrison, 2008).

Overall, the retrieved sources are often characterised by mixed chemical properties; this was partially expected due to the high residence times of PM_1 (higher than 1 day for fine aerosols in the Po Valley, as estimated by Crova et al., 2021) and the reprocessing of atmospheric aerosol favoured by the poor atmospheric dilution typical of the Po Valley. Moreover, it is also worth stressing that PM_1 features - in terms of concentrations, composition, and emissions - can be different than usual since lockdown stringency measures were still active (especially during the winter campaign) to limit the spread of COVID-19 pandemic.

3.3. Dispersion normalised multi-time resolution model results

3.3.1. DN-MT versus REG-MT

As already mentioned, the aim of this work was to explore the potentiality of the dispersion-normalised multi-time approach (DN-MT) to better comprehend the causes of high PM levels in the Po Valley by disentangling the effects of poor atmospheric dilution from emissions.

By exploiting the availability of MLH estimates and mean wind speed data, DN-MT was run and a 5-factor solution (minimum Q = Q_{main} +

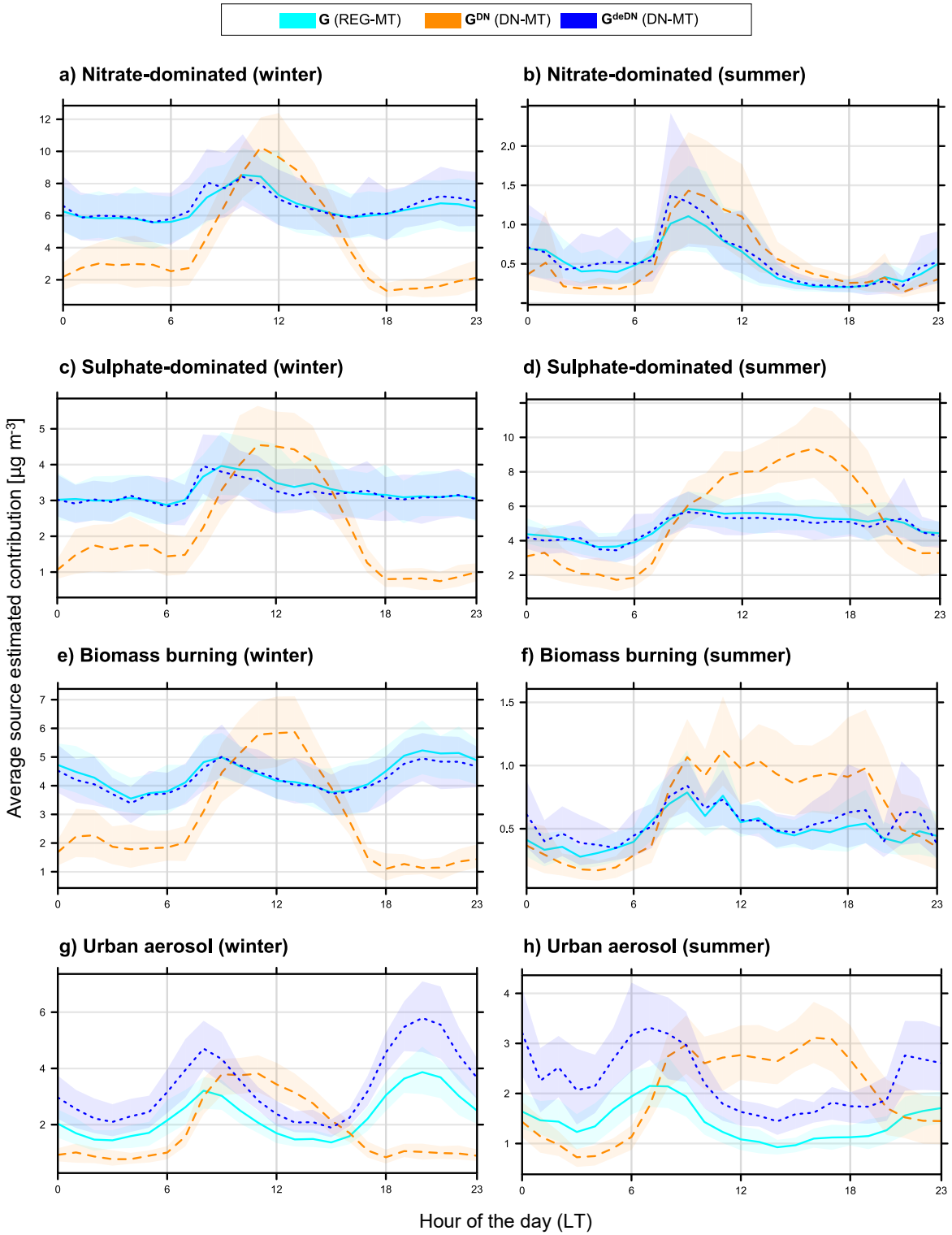

Fig. 4. Factors diel variations. Cyan solid lines: diel profiles from **G** matrix (REG-MT). Orange dashed lines: diel profiles from $\mathbf{G}^{\mathbf{DN}}$ matrix (DN-MT). Blue dotted lines: diel profiles from $\mathbf{G}^{\mathbf{deDN}}$ matrix (DN-MT). Left panels (a,c,e,g): winter diel variations. Right panels (b,d,f,h): summer diel variations. Lines represent mean values, shaded areas are the 95% confidence interval in the mean ('openair' package, Carslaw, 2013; Carslaw and Ropkins, 2012; R Core Team, 2021). Diel variations of the episodic contributions from the mineral dust factor are not displayed as not meaningful.

Q_{aux} = 8435) was selected; indeed, it was consistent with REG-MT outcomes and the solution consistency and robustness was checked with satisfactory results. It is important to recall that in DN-MT the source-to-factor assignments are the same as REG-MT, while differences are related to source temporal patterns and contributions which might be impacted by the atmospheric dilution conditions.

Indeed, as can be noted from Fig. 2, SF5, and SF6 factor chemical profiles given by the $\mathbf{F}^{\mathbf{DN}}$ matrix and EVF values in the DN-MT approach are overall very similar to the ones provided by the REG-MT, as expected. Diel variations are reported in Fig. 4 (panels a-h) for all the

factors retrieved by the model (except for the mineral dust factor since diel variation are dominated by the Saharan dust transport episodes and thus are not significant).

In Table 2, average (mean [95% CI]) absolute and percentage source contributions are reported for winter and summer; they were computed by averaging **G** matrix temporal series obtained by both REG- and DN-MT approach. The percentage difference was calculated as (DN-MT – REG-MT)/REG-MT using the mass contribution apportioned by the two approaches. It is important to remember that here the DN-MT results refer to the de-normalised matrix $\mathbf{G^{deDN}}$ because - as reported in Section 2.2.2 - a de-normalisation of the g_{ik}^{DN} values must be applied to the output values to keep the consistency with the measured ambient PM concentrations.

The similarity between the factor contributions obtained by REG- and DN-MT is particularly evident for the secondary aerosol related ones (i.e. nitrate- and sulphate-dominated) and the biomass burning, with percentage differences in the major contributing species in the mass-scaled profiles are smaller than 4%. Opposite, statistically different values were observed for mineral dust and for urban aerosol. The similarity among the chemical profiles (see Fig. 2) retrieved with the REG- and DN-MT suggests that source identification and the contributions quantification performed in this study are robust and reliable.

Time series of factor contributions obtained by the de-normalised matrix $\mathbf{G^{deDN}}$ in the DN-MT are almost overlapping (at 95% CI) with those given by the **G** matrix in the REG-MT for secondary aerosol-dominated factors and biomass burning; differences between the two approaches are not statistically significant. Indeed, nitrate and sulphate aerosol mixtures originate from multiple atmospheric processes and reactions on different time scales; moreover, in the Po Valley the secondary aerosol production is largely observed at a regional scale (i.e., basin-based). The same behaviour was observed for biomass burning diel patterns, which did not seem to be affected by the VC-normalisation. The non-local character of these factors was also confirmed by the Conditional Probability Function (CPF) plots (see Figs. S2, S3, and S4) which showed that for these factors the contributions are never coming from the city (located to the south of the investigated site); opposite, they are coming from the north-western sector, indicating that these contributions are originated in the Po Valley basin.

As concerns the other factors, the DN-MT time patterns are very similar to the REG-MT ones but with different average contributions. Mineral dust contribution is more largely decreased in winter of about 23% while remains comparable during summer. The urban aerosol factor is the one experiencing the larger variation with the DN-MT approach, its contribution being increased by about 46% and 59% in winter and summer, respectively; moreover, it is the only factor with the non-overlapping contributions at 95% CI. This is also very clear considering diel variation patterns, where peaks likely due to traffic-rush hours present in the urban factor are strongly enhanced (Fig. 4g and h), while mineral dust pattern is flattened especially in winter after the VC-normalisation (not shown). In our work, secondary aerosol components (i.e. mainly nitrate- and sulphate-dominated aerosol) together with biomass burning temporal patterns are not expected to be so much affected by atmospheric dilution and local meteorology. Such results are in accordance with what was observed in other works (Dai et al., 2020; Sofowote et al., 2021), where peaks of primary emissions related to local sources (e.g., traffic) were sharpened by the DN approach, while contributions from non-local sources (e.g., soil dust and sea salt) were lowered.

3.3.2. *Interpretation of G^{DN} matrix results*

The temporal patterns given by the $\mathbf{G^{DN}}$ matrix, giving information about the actual emission strength (including possible atmospheric chemical transformations) of the identified sources independently from atmospheric dilution effects, were analysed in detail, as an original contribution to future DN-PMF applications. These outputs exhibit strongly modulated patterns for all the sources in both seasons (Fig. 3) and the minimum values are set to almost constant values. By comparing **G** and $\mathbf{G^{deDN}}$ patterns with $\mathbf{G^{DN}}$, it is very straightforward to identify the periods where **G** and $\mathbf{G^{deDN}}$ concentration increase is mainly caused by PM accumulation due to atmospheric stability as can be clearly seen during periods 1-8 and 17–23 February, which correspond to very poor dilution conditions as indicated by the very low VC values (see Fig. 1). Considering diel variations (Fig. 4, panels a-h), it can be noted that almost all the sources are majorly active during diurnal hours. The common features shown by sulphate- and nitrate-dominated aerosol as well as by biomass burning suggest that the slow modulation of regional-based emissions in the DN-MT is masked by the strong daily evolution of the mixing layer which overwhelms any other variation in these factors; indeed, the $\mathbf{G^{DN}}$ shape resembles very much the MLH one.

In winter, secondary aerosol factors are characterised by a very similar diel pattern, presenting a maximum around 11:00, about 4 h after the sunrise (typically occurring around 7:00 during the winter campaign); this morning peak is likely due to an enhancement of photochemical reactions in the first hours of solar radiation (Dai et al., 2020). During summer, the patterns of these sources are different. The nitrate-dominated factor, similarly to wintertime behaviour, has a peak around 9:00, about 3–4 h after the sunrise (occurring on average at around 5:30 during the summer campaign); the concentrations then drop due to higher temperatures which favour the gaseous form. The sulphate-dominated factor reaches its maximum later in the afternoon at about 16:00 when high photochemical activity promotes the formation of sulphate. This factor in summer is the one exhibiting the most strongly modulated pattern. Biomass burning showed a very similar diurnal variation to nitrate- and sulphate-dominated factors in winter, with a peak slightly shifted forward at about 13:00 and an additional smaller peak during nocturnal hours around 1:00–2:00. This pattern was quite unexpected since biomass burning emissions are typically more intense during night-time, when there is an increased use of biomass combustion for residential heating. The features retrieved in this analysis emphasise the complexity of this source. Indeed, biomass burning is mainly traced by species typically emitted directly into the atmosphere (e.g., levoglucosan and EC), but the high similarity with secondary aerosol-dominated factors highlighted by the DN-MT suggests a prevailing regional and secondary origin. This could be explained by considering that biomass burning emissions are subjected to rapid processing and ageing once released in the atmosphere (as reported by e.g., Kodros et al., 2020; Paglione et al., 2020); this is often promoted by wintertime conditions typical of the Po Valley when high concentration levels and scarce dilution produce a complex mixture of pollutants. During summer, biomass burning contribution is almost negligible so that it is not of interest commenting on it.

As already mentioned, the observed diel variation of regional emissions is heavily affected by the MLH modulation; however in this case different biomass burning temporal patterns might also originate from lockdown measures that were still active during the winter field campaign and forced people to stay at home during daytime thus increasing the use of biomass burning for heating. It is noteworthy that a different behaviour was observed for the urban factor, which has a local origin. In winter, the urban factor was characterised by a sharp morning rise till maximum values in the time interval 9:00–11:00, followed by a slow decrease towards late afternoon at about 18:00. In summer, it was mainly active during the central hours of the day (8:00–18:00), with two peaks (one in the morning around 9:00 and in the evening around 16:00–17:00). Hourly traffic volumes measured by the municipality of BO on a road which is not too far from our urban background monitoring site were downloaded from open data archives (Open Data – Comune di Bologna, https://opendata.comune.bologna.it, last visited on 10 March 2023) and compared to the urban factor diel variations. It is very interesting to note that during summer, the urban factor diel variation shows a very good agreement with diel traffic volume ($R^2 = 0.88$, see Figure SF7), even if the evening peak was slightly before the one

presented in the traffic volume. The same agreement was not found in winter, when although the traffic volume pattern behaved similarly to the summer one (even if with lower absolute values) the temporal pattern of the urban factor contributions completely missed the evening peak. This behaviour might be explained by considering that particles emitted by this emission source in wintertime conditions (i.e., frequent atmospheric stability conditions with high relative humidity, complexity of the mixture of gaseous and particulate pollutants) can undertake transformations that modify their nature, such as mixing with other existing particles, water vapour condensation upon particles, or ageing processes and it might be that these particles increase their size so that PM_1 sampling inlet did not catch them.

Lastly, mineral dust patterns (not shown) are dominated by the Saharan dust transport episodes; however, apart from those events, the diel pattern is characterised by daily peaks around 11:00–13:00 in winter and around 17:00–18:00 in summer, likely because the wind speed is maximum in those hours of the day (see Figure SF2d).

4. Conclusions

In this work, we explored the potentiality of DN-PMF in decoupling the effect of atmospheric dispersion from aerosol emission sources and atmospheric chemistry in the southern Po Valley, one of the major pollution hotspots in Europe. Indeed, it is worth assessing how much the strong atmospheric stability drives the observed atmospheric aerosol concentrations vs. the emission source strengths as this piece of information is key for air quality improvement plans. This is the first application of DN-MT at a European site where meteorological conditions play a crucial role in atmospheric aerosol concentrations.

To achieve this goal, a dataset comprising PM_1 well chemically characterised samples with multiple-time resolution was chosen as a challenging input for receptor modelling due to the relatively long residence time in the atmosphere of sub-micron sized particles and the huge contributions from secondary components of regional origin. These are features that make the Po Valley aerosol so complex and worthy of investigation. In addition, the monitoring campaigns were carried out when source emissions were not as usual because of some restrictions due to COVID-19 pandemics.

The application of DN-MT to this dataset compared to the more conventional use of REG-MT pointed out some interesting features when looking at the differences in high-time resolution and diel patterns. The similarity observed for sulphate- and nitrate-dominated aerosol as well as for biomass burning revealed their regional origin as the DN-MT outputs ($\mathbf{G}^{\mathbf{DN}}$) show a pattern which resembles the mixing layer evolution thus suggesting that the latter dominates over the relatively slow modulation of components which are largely produced at the basin-scale of the Po Valley. Opposite, the urban aerosol - in this case the only source with a local origin - shows $\mathbf{G}^{\mathbf{DN}}$ values which appear to be much more related to the modulation of the emission source (like traffic volumes, in this case).

As a perspective of this work, further studies applying the DN-PMF using datasets with different PM size fractions from the Po Valley are desirable to gain knowledge about the potentiality of this approach in retrieving useful information on the role of the atmospheric dilution on the observed concentrations to better tackle the pollution levels and to promote more effective abatement strategies.

Funding

This work was supported by the Italian Ministry of the University (MUR) with the PRIN2017 grant for the RHAPS project [grant number: 2017MSN7M8].

CRediT authorship contribution statement

Federica Crova: Formal analysis, Investigation, Methodology, Visualization, Writing – original draft, Writing – review & editing. **Alice Corina Forello:** Formal analysis, Investigation, Writing – review & editing. **Vera Bernardoni:** Data curation, Validation, Investigation. **Giulia Calzolai:** Data curation, Validation. **Silvia Canepari:** Investigation, Writing – review & editing. **Stefania Argentini:** Data curation. **Francesca Costabile:** Data curation, Investigation, Writing – review & editing. **Maria Agostina Frezzini:** Investigation, Writing – review & editing. **Fabio Giardi:** Data curation, Investigation. **Franco Lucarelli:** Data curation, Funding acquisition, Investigation. **Dario Massabò:** Data curation, Funding acquisition, Investigation. **Lorenzo Massimi:** Data curation, Investigation, Writing – review & editing. **Silvia Nava:** Data curation, Validation. **Marco Paglione:** Formal analysis, Investigation, Methodology, Writing – original draft, Writing – review & editing. **Giulia Pazzi:** Data curation, Investigation. **Paolo Prati:** Funding acquisition, Investigation. **Matteo Rinaldi:** Formal analysis, Investigation, Methodology, Visualization, Writing – review & editing. **Mara Russo:** Investigation. **Sara Valentini:** Data curation, Investigation, Validation, Writing – review & editing. **Gianluigi Valli:** Data curation, Investigation, Methodology, Validation, Writing – review & editing. **Virginia Vernocchi:** Data curation, Investigation, Validation. **Roberta Vecchi:** Conceptualization, Funding acquisition, Investigation, Methodology, Supervision, Writing – original draft, Writing – review & editing.

Declaration of competing interest

The authors declare that they have no known competing financial interests or personal relationships that could have appeared to influence the work reported in this paper.

Data availability

Data will be made available on request.

Acknowledgements

The authors are grateful to all the RHAPS collaborators for the support during field campaigns, data validation and data analysis; to Patrizia Favaron and Sara Lucherini for MLH estimates; to Philip K. Hopke, Uwayemi M. Sofowote, and Dennis Mooibroek for the useful discussions about DISP implementation.

Appendix A. Supplementary data

Supplementary data to this article can be found online at https://doi.org/10.1016/j.atmosenv.2023.120168.

References

Amato, F., Alastuey, A., Karanasiou, A., Lucarelli, F., Nava, S., Calzolai, G., Severi, M., Becagli, S., Gianelle, V.L., Colombi, C., Alves, C., Custódio, D., Nunes, T., Cerqueira, M., Pio, C., Eleftheriadis, K., Diapouli, E., Reche, C., Minguillón, M.C., Manousakas, M.I., Maggos, T., Vratolis, S., Harrison, R.M., Querol, X., 2016. AIRUSE-LIFE+: a harmonized PM speciation and source apportionment in five southern European cities. Atmos. Chem. Phys. 16, 3289–3309. https://doi.org/10.5194/acp-16-3289-2016.

Amato, F., Pandolfi, M., Escrig, A., Querol, X., Alastuey, A., Pey, J., Perez, N., Hopke, P. K., 2009. Quantifying road dust resuspension in urban environment by Multilinear Engine: a comparison with PMF2. Atmos. Environ. 43, 2770–2780. https://doi.org/10.1016/j.atmosenv.2009.02.039.

Anttila, P., Makkonen, U., Hellén, H., Kyllönen, K., Leppänen, S., Saari, H., Hakola, H., 2008. Impact of the open biomass fires in spring and summer of 2006 on the chemical composition of background air in south-eastern Finland. Atmos. Environ. 42, 6472–6486. https://doi.org/10.1016/j.atmosenv.2008.04.020.

Bernardoni, V., Vecchi, R., Valli, G., Piazzalunga, A., Fermo, P., 2011. PM10 source apportionment in Milan (Italy) using time-resolved data. Sci. Total Environ. 409 (22), 4788–4795. https://doi.org/10.1016/j.scitotenv.2011.07.048.

Bauer, D.F., 1972. Constructing confidence sets using rank statistics. J. Am. Stat. Assoc. 67, 687–690. https://doi.org/10.2307/2284469.

Brown, S.G., Eberly, S., Paatero, P., Norris, G.A., 2015. Methods for estimating uncertainty in PMF solutions: examples with ambient air and water quality data and

guidance on reporting PMF results. Sci. Total Environ. 518–519, 626–635. https://doi.org/10.1016/j.scitotenv.2015.01.022.
Calzolai, G., Lucarelli, F., Chiari, M., Nava, S., Giannoni, M., Carraresi, L., Prati, P., Vecchi, R., 2015. Improvements in PIXE analysis of hourly particulate matter samples. Nucl. Instrum. Methods Phys. Res. Sect. B Beam Interact. Mater. Atoms 363, 99–104. https://doi.org/10.1016/j.nimb.2015.08.022.
Canagaratna, M.R., Jayne, J.T., Jimenez, J.L., Allan, J.D., Alfarra, M.R., Zhang, Q., Onasch, T.B., Drewnick, F., Coe, H., Middlebrook, A., Delia, A., Williams, L.R., Trimborn, A.M., Northway, M.J., DeCarlo, P.F., Kolb, C.E., Davidovits, P., Worsnop, D.R., 2007. Chemical and microphysical characterization of ambient aerosols with the aerodyne aerosol mass spectrometer. Mass Spectrom. Rev. 26, 185–222. https://doi.org/10.1002/mas.20115.
Carslaw, D.C., 2013. The Openair Manual — Open-Source Tools for Analyzing Air Pollution Data. Manual for Version 0.8-0.
Carslaw, D.C., Ropkins, K., 2012. Openair — an R Package for Air Quality Data Analysis, 27–28. Environmental Modelling & Software: With Environment Data News, pp. 52–61.
Chen, Y., Masiol, M., Squizzato, S., Chalupa, D.C., Zíková, N., Pokorná, P., Rich, D.Q., Hopke, P.K., 2022a. Long-term trends of ultrafine and fine particle number concentrations in New York State: apportioning between emissions and dispersion. Environ. Pollut. 310 https://doi.org/10.1016/j.envpol.2022.119797.
Chen, Y., Rich, D.Q., Hopke, P.K., 2022b. Long-term PM2.5 source analyses in New York City from the perspective of dispersion normalized PMF. Atmos. Environ. 272, 118949 https://doi.org/10.1016/j.atmosenv.2022.118949.
Costabile, F., Alas, H., Aufderheide, M., Avino, P., Amato, F., Argentini, S., Barnaba, F., Berico, M., Bernardoni, V., Biondi, R., Calzolai, G., Canepari, S., Casasanta, G., Ciampichetti, S., Conidi, A., Cordelli, E., Ianni, A. Di, Liberto, L.Di, Facchini, M.C., Facci, A., Frasca, D., Gilardoni, S., Grollino, M.G., Gualtieri, M., Lucarelli, F., Malaguti, A., Manigrasso, M., Montagnoli, M., Nava, S., Padoan, E., Perrino, C., Petralia, E., Petenko, I., Querol, X., Simonetti, G., Tranfo, G., Ubertini, S., Valli, G., Valentini, S., Vecchi, R., Volpi, F., Weinhold, K., Wiedensholer, A., Zanini, G., Gobbi, G.P., 2017. First results of the "carbonaceous aerosol in Rome and environs (CARE)" experiment: beyond current standards for PM10. Atmosphere 8. https://doi.org/10.3390/atmos8120249.
Costabile, F., Decesari, S., Vecchi, R., Lucarelli, F., Curci, G., Massabò, D., Rinaldi, M., Gualtieri, M., Corsini, E., Menegola, E., Canepari, S., Massimi, L., Argentini, S., Busetto, M., Di Iulio, G., Di Liberto, L., Paglione, M., Petenko, I., Russo, M., Marinoni, A., Casasanta, G., Valentini, S., Bernardoni, V., Crova, F., Valli, G., Forello, A.C., Giardi, F., Nava, S., Pazzi, G., Prati, P., Vernocchi, V., La Torretta, T., Petralia, E., Stracquadanio, M., Zanini, G., Melzi, G., Nozza, E., Iulini, M., Caruso, D., Cioffi, L., Imperato, G., Giavarini, F., Battistoni, M., Di Renzo, F., Frezzini, M.A., Perrino, C., Facchini, M.C., 2022. On the redox-activity and health-effects of atmospheric primary and secondary aerosol: phenomenology. Atmosphere 13. https://doi.org/10.3390/atmos13050704.
Crespi, A., Bernardoni, V., Calzolai, G., Lucarelli, F., Nava, S., Valli, G., Vecchi, R., 2016. Implementing constrained multi-time approach with bootstrap analysis in ME-2: an application to PM2.5 data from Florence (Italy). Sci. Total Environ. 541, 502–511. https://doi.org/10.1016/j.scitotenv.2015.08.159.
Crosier, J., Allan, J.D., Coe, H., Bower, K.N., Formenti, P., Williams, P.I., 2007. Chemical composition of summertime aerosol in the Po valley (Italy), northern adriatic and black sea. Q. J. R. Meteorol. Soc. 133, 61–75. https://doi.org/10.1002/qj.88.
Crova, F., Valli, G., Bernardoni, V., Forello, A.C., Valentini, S., Vecchi, R., 2021. Effectiveness of airborne radon progeny assessment for atmospheric studies. Atmos. Res. 250, 105390 https://doi.org/10.1016/j.atmosres.2020.105390.
D'Alessandro, A., Lucarelli, F., Mandò, P.A., Marcazzan, G., Nava, S., Prati, P., Valli, G., Vecchi, R., Zucchiatti, A., 2003. Hourly elemental composition and sources identification of fine and coarse PM10 particulate matter in four Italian towns. J. Aerosol Sci. 34, 243–259. https://doi.org/10.1016/S0021-8502(02)00172-6.
Dai, Q., Ding, J., Song, C., Liu, B., Bi, X., Wu, J., Zhang, Y., Feng, Y., Hopke, P.K., 2021. Changes in source contributions to particle number concentrations after the COVID-19 outbreak: insights from a dispersion normalized PMF. Sci. Total Environ. 759, 143548 https://doi.org/10.1016/j.scitotenv.2020.143548.
Dai, Q., Liu, B., Bi, X., Wu, J., Liang, D., Zhang, Y., Feng, Y., Hopke, P.K., 2020. Dispersion normalized PMF provides insights into the significant changes in source contributions to PM2.5 after the COVID-19 outbreak. Environ. Sci. Technol. 54, 9917–9927. https://doi.org/10.1021/acs.est.0c02776.
EEA, 2019. Air Quality in Europe—2019 Report. Copenhagen, Denmark.
Farao, C., Canepari, S., Perrino, C., Harrison, R.M., 2014. Sources of PM in an industrial area: comparison between receptor model results and semiempirical calculations of source contributions. Aerosol Air Qual. Res. 14, 1558–1572. https://doi.org/10.4209/aaqr.2013.08.0281.
Forello, A.C., Amato, F., Bernardoni, V., Calzolai, G., Canepari, S., Costabile, F., Di Liberto, L., Gualtieri, M., Lucarelli, F., Nava, S., Perrino, C., Petralia, E., Valentini, S., Valli, G., Vecchi, R., 2020. Gaining knowledge on source contribution to aerosol optical absorption properties and organics by receptor modelling. Atmos. Environ. 243, 117873 https://doi.org/10.1016/j.atmosenv.2020.117873.
Forello, A.C., Bernardoni, V., Calzolai, G., Lucarelli, F., Massabò, D., Nava, S., Pileci, R.E., Prati, P., Valentini, S., Valli, G., Vecchi, R., 2019. Exploiting multi-wavelength aerosol absorption coefficients in a multi-time resolution source apportionment study to retrieve source-dependent absorption parameters. Atmos. Chem. Phys. 19, 11235–11252. https://doi.org/10.5194/acp-19-11235-2019.
Gu, Y., Liu, B., Dai, Q., Zhang, Y., Zhou, M., Feng, Y., Hopke, P.K., 2022. Multiply improved positive matrix factorization for source apportionment of volatile organic compounds during the COVID-19 shutdown in Tianjin, China. Environ. Int. 158, 106979 https://doi.org/10.1016/j.envint.2021.106979.
Hansen, H.K., Pedersen, A.J., Ottosen, L.M., Villumsen, A., 2001. Speciation and mobility of cadmium in straw and wood combustion fly ash. Chemosphere 45 (1), 123–128.
HealthEffectsInstitute, 2020. State of Global Air 2020: A Special Report on Global Exposure to Air Pollution and its Health Impacts, vol. 2020. Health Effects Institute, Institute for Health Metrics and Evaluation. https://www.stateofglobalair.org.
Hennigan, C.J., Sullivan, A.P., Collett, J.L., Robinson, A.L., 2010. Levoglucosan stability in biomass burning particles exposed to hydroxyl radicals. Geophys. Res. Lett. 37, 2–5. https://doi.org/10.1029/2010GL043088.
Hovorka, J., Pokorná, P., Hopke, P.K., Křůmal, K., Mikuška, P., Píšová, M., 2015. Wood combustion, a dominant source of winter aerosol in residential district in proximity to a large automobile factory in Central Europe. Atmos. Environ. 113, 98–107. https://doi.org/10.1016/j.atmosenv.2015.04.068.
IPCC, 2021. Climate Change 2021: the Physical Science Basis. Contribution of Working Group I to the Sixth Assessment Report of the Intergovernmental Panel on Climate Change. Cambridge University Press, Cambridge, United Kingdom and New York, NY, USA.
Kim, E., Hopke, P.K., Edgerton, E.S., 2003. Source identification of Atlanta aerosol by positive matrix factorization. J. Air Waste Manag. Assoc. 53, 731–739. https://doi.org/10.1080/10473289.2003.10466209.
Kim, Y., Jeon, K., Park, J., Shim, K., Kim, S.W., Shin, H.J., Yi, S.M., Hopke, P.K., 2022. Local and transboundary impacts of PM2.5 sources identified in Seoul during the early stage of the COVID-19 outbreak. Atmos. Pollut. Res. 13, 101510 https://doi.org/10.1016/j.apr.2022.101510.
Kodros J.K., Papanastasiou D.K., Paglione M., Masiol M., Squizzato S., Florou K., Skyllakou K., Kaltsonoudis C., Nenes A., Pandis S.N. Rapid dark aging of biomass burning as an overlooked source of oxidized organic aerosol. Proc. Natl. Acad. Sci. U. S.A. 117, 33028-33033. https://doi.org/10.1073/pnas.2010365117.
Kuo, C.P., Liao, H.T., Chou, C.C.K., Wu, C.F., 2014. Source apportionment of particulate matter and selected volatile organic compounds with multiple time resolution data. Sci. Total Environ. 472, 880–887. https://doi.org/10.1016/j.scitotenv.2013.11.114.
Larsen, B.R., Gilardoni, S., Stenström, K., Niedzialek, J., Jimenez, J., Belis, C.A., 2012. Sources for PM air pollution in the Po Plain, Italy: II. Probabilistic uncertainty characterization and sensitivity analysis of secondary and primary sources. Atmos. Environ. 50, 203–213. https://doi.org/10.1016/j.atmosenv.2011.12.038.
Lelieveld, J., Evans, J.S., Fnais, M., Giannadaki, D., Pozzer, A., 2015. The contribution of outdoor air pollution sources to premature mortality on a global scale. Nature 525, 367–371. https://doi.org/10.1038/nature15371.
Li, W., Ge, P., Chen, M., Tang, J., Cao, M., Cui, Y., Hu, K., Nie, D., 2021. Tracers from biomass burning emissions and identification of biomass burning. Atmosphere 12. https://doi.org/10.3390/atmos12111401.
Liao, H.T., Chou, C.C.K., Chow, J.C., Watson, J.G., Hopke, P.K., Wu, C.F., 2015. Source and risk apportionment of selected VOCs and PM2.5 species using partially constrained receptor models with multiple time resolution data. Environ. Pollut. 205, 121–130. https://doi.org/10.1016/j.envpol.2015.05.035.
Lucarelli, F., Calzolai, G., Chiari, M., Giannoni, M., Mochi, D., Nava, S., Carraresi, L., 2014. The upgraded external-beam PIXE/PIGE set-up at LABEC for very fast measurements on aerosol samples. Nucl. Instrum. Methods Phys. Res. Sect. B Beam Interact. Mater. Atoms 318, 55–59. https://doi.org/10.1016/j.nimb.2013.05.099.
Marcazzan, G.M., Ceriani, M., Valli, G., Vecchi, R., 2004. Composition, components and sources of fine aerosol fractions using multielemental EDXRF analysis. X Ray Spectrom. 33, 267–272. https://doi.org/10.1002/xrs.719.
Masiol, M., Squizzato, S., Rampazzo, G., Pavoni, B., 2014. Source apportionment of PM2.5 at multiple sites in Venice (Italy): spatial variability and the role of weather. Atmos. Environ. 98, 78–88. https://doi.org/10.1016/j.atmosenv.2014.08.059.
Masiol, M., Squizzato, S., Formenton, G., Khan, M.B., Hopke, P.K., Nenes, A., Pandis, S. N., Tositti, L., Benetello, F., Visin, F., Pavoni, B., 2020. Hybrid multiple-site mass closure and source apportionment of PM2.5 and aerosol acidity at major cities in the Po Valley. Sci. Total Environ. 704, 135287 https://doi.org/10.1016/j.scitotenv.2019.135287.
Mason, B., 1966. Principles of Geochemistry. Wiley and Sons, New York.
Mooibroek, D., Sofowote, U.M., Hopke, P.K., 2022. Source apportionment of ambient PM10 collected at three sites in an urban-industrial area with multi-time resolution factor analyses. Sci. Total Environ. 850, 157981 https://doi.org/10.1016/j.scitotenv.2022.157981.
Narodoslawsky, M., Obernberger, I., 1996. From waste to raw material—the route from biomass to wood ash for cadmium and other heavy metals. J. Hazard Mater. 50 (2–3), 157–168. https://doi.org/10.1016/0304-3894(96)01785-2.
Norris, G., Duvall, S., Brown, S., Bai, S., 2014. EPA Positive Matrix Factorization (PMF) 5.0. Fundamentals and User Guide. EPA/600/R-14/108 (NTIS PB2015-105147).
Nozza, E., Valentini, S., Melzi, G., Vecchi, R., Corsini, E., 2021. Advances on the immunotoxicity of outdoor particulate matter: a focus on physical and chemical properties and respiratory defence mechanisms. Sci. Total Environ. 780, 146391 https://doi.org/10.1016/j.scitotenv.2021.146391.
Ogulei, D., Hopke, P.K., Zhou, L., Paatero, P., Park, S.S., Ondov, J.M., 2005. Receptor modeling for multiple time resolved species: the Baltimore supersite. Atmos. Environ. 39, 3751–3762. https://doi.org/10.1016/j.atmosenv.2005.03.012.
Ozgen, S., Becagli, S., Bernardoni, V., Caserini, S., Caruso, D., Corbella, L., Dell'Acqua, M., Fermo, P., Gonzalez, R., Lonati, G., Signorini, S., Tardivo, R., Tosi, E., Valli, G., Vecchi, R., Marinovich, M., 2017. Analysis of the chemical composition of ultrafine particles from two domestic solid biomass fired room heaters under simulated real-world use. Atmos. Environ. 150, 87–97. https://doi.org/10.1016/j.atmosenv.2016.11.048.
Paatero, P., 2012. The Multilinear Engine (ME-2) Script Language (V. 1.352), Available with the Program ME-2 (me2scrip.Txt).
Paatero, P., 1999. The multilinear engine—a table-driven, least squares program for solving multilinear problems, including the n-way parallel factor analysis model.

J. Comput. Graph Stat. 8, 854–888. https://doi.org/10.1080/10618600.1999.10474853.
Paatero, P., Eberly, S., Brown, S.G., Norris, G.A., 2014. Methods for estimating uncertainty in factor analytic solutions. Atmos. Meas. Tech. 7, 781–797. https://doi.org/10.5194/amt-7-781-2014.
Paatero, P., Hopke, P.K., Begum, B.A., Biswas, S.K., 2005. A graphical diagnostic method for assessing the rotation in factor analytical models of atmospheric pollution. Atmos. Environ. 39, 193–201. https://doi.org/10.1016/j.atmosenv.2004.08.018.
Paglione, M., Gilardoni, S., Rinaldi, M., Decesari, S., Zanca, N., Sandrini, S., Giulianelli, L., Bacco, D., Ferrari, S., Poluzzi, V., Scotto, F., Trentini, A., Poulain, L., Herrmann, H., Wiedensohler, A., Canonaco, F., Prévôt, A.S.H., Massoli, P., Carbone, C., Facchini, M.C., Fuzzi, S., 2020. The impact of biomass burning and aqueous-phase processing on air quality: a multi-year source apportionment study in the Po Valley, Italy. Atmos. Chem. Phys. 20, 1233–1254. https://doi.org/10.5194/acp-20-1233-2020.
Park, J., Kim, H., Kim, Y., Heo, J., Kim, S.W., Jeon, K., Yi, S.M., Hopke, P.K., 2022. Source apportionment of PM2.5 in Seoul, South Korea and Beijing, China using dispersion normalized PMF. Sci. Total Environ. 833, 155056 https://doi.org/10.1016/j.scitotenv.2022.155056.
Piazzalunga, A., Bernardoni, V., Fermo, P., Vecchi, R., 2013. Optimisation of analytical procedures for the quantification of ionic and carbonaceous fractions in the atmospheric aerosol and applications to ambient samples. Anal. Bioanal. Chem. 405, 1123–1132. https://doi.org/10.1007/s00216-012-6433-5.
Piazzalunga, A., Fermo, P., Bernardoni, V., Vecchi, R., Valli, G., De Gregorio, M.A., 2010. A simplified method for levoglucosan quantification in wintertime atmospheric particulate matter by high performance anion-exchange chromatography coupled with pulsed amperometric detection. Int. J. Environ. Anal. Chem. 90, 934–947. https://doi.org/10.1080/03067310903023619.
Polissar, A.V., Hopke, P.K., Paatero, P., Malm, W.C., Sisler, J.F., 1998. J. Geophys. Res. 103 (19) https://doi.org/10.1029/98JD01212, 045-19,057.
Putaud, J.P., Van Dingenen, R., Alastuey, A., Bauer, H., Birmili, W., Cyrys, J., Flentje, H., Fuzzi, S., Gehrig, R., Hansson, H.C., Harrison, R.M., Herrmann, H., Hitzenberger, R., Hüglin, C., Jones, A.M., Kasper-Giebl, A., Kiss, G., Kousa, A., Kuhlbusch, T.A.J., Löschau, G., Maenhaut, W., Molnar, A., Moreno, T., Pekkanen, J., Perrino, C., Pitz, M., Puxbaum, H., Querol, X., Rodriguez, S., Salma, I., Schwarz, J., Smolik, J., Schneider, J., Spindler, G., ten Brink, H., Tursic, J., Viana, M., Wiedensohler, A., Raes, F., 2010. A European aerosol phenomenology - 3: physical and chemical characteristics of particulate matter from 60 rural, urban, and kerbside sites across Europe. Atmos. Environ. 44, 1308–1320. https://doi.org/10.1016/j.atmosenv.2009.12.011.
R Core Team, 2021. R: A Language and Environment for Statistical Computing. R Foundation for Statistical Computing, Vienna, Austria. https://www.R-project.org/.
Ricciardelli, I., Bacco, D., Rinaldi, M., Bonafè, G., Scotto, F., Trentini, A., Bertacci, G., Ugolini, P., Zigola, C., Rovere, F., Maccone, C., Pironi, C., Poluzzi, V., 2017. A three-year investigation of daily PM2.5 main chemical components in four sites: the routine measurement program of the Supersito Project (Po Valley, Italy). Atmos. Environ. 152, 418–430. https://doi.org/10.1016/j.atmosenv.2016.12.052.
Scotto, F., Bacco, D., Lasagni, S., Trentini, A., Poluzzi, V., Vecchi, R., 2021. A multi-year source apportionment of PM2.5 at multiple sites in the southern Po Valley (Italy). Atmos. Pollut. Res. 12, 101192 https://doi.org/10.1016/j.apr.2021.101192.
Seinfeld, J.H., Pandis, S.N., 2016. Atmospheric Chemistry and Physics: from Air Pollution to Climate Change, third ed. John Wiley & Sons.
Sofowote, U.M., Healy, R.M., Su, Y., Debosz, J., Noble, M., Munoz, A., Jeong, C.-H., Wang, J.M., Hilker, N., Evans, G.J., Hopke, P.K., 2018. Understanding the PM2.5 imbalance between a far and near-road location: results of high temporal frequency source apportionment and parameterization of black carbon. Atmos. Environ. 173, 277–288. https://doi.org/10.1016/J.ATMOSENV.2017.10.063.
Sofowote, U.M., Healy, R.M., Su, Y., Debosz, J., Noble, M., Munoz, A., Jeong, C.H., Wang, J.M., Hilker, N., Evans, G.J., Brook, J.R., Lu, G., Hopke, P.K., 2021. Sources, variability and parameterizations of intra-city factors obtained from dispersion-normalized multi-time resolution factor analyses of PM2.5 in an urban environment. Sci. Total Environ. 761 https://doi.org/10.1016/j.scitotenv.2020.143225.
Sofowote, U.M., Mooibroek, D., Healy, R.M., Debosz, J., Munoz, A., Hopke, P.K., 2023. Source apportionment of ambient PM2.5 in an industrialized city using dispersion-normalized, multi-time resolution factor analyses. Environ. Pollut. 323, 121281 https://doi.org/10.1016/j.envpol.2023.121281.
Squizzato, S., Masiol, M., Agostini, C., Visin, F., Formenton, G., Harrison, R.M., Rampazzo, G., 2016. Factors, origin and sources affecting PM1 concentrations and composition at an urban background site. Atmos. Res. 180, 262–273. https://doi.org/10.1016/j.atmosres.2016.06.002.
Squizzato, S., Masiol, M., Brunelli, A., Pistollato, S., Tarabotti, E., Rampazzo, G., Pavoni, B., 2013. Factors determining the formation of secondary inorganic aerosol: a case study in the Po Valley (Italy). Atmos. Chem. Phys. 13, 1927–1939. https://doi.org/10.5194/acp-13-1927-2013.
Srivastava, D., Favez, O., Petit, J.-E., Zhang, Y., Sofowote, U.M., Hopke, P.K., Bonnaire, N., Perraudin, E., Gros, V., Villenave, E., Albinet, A., 2019. Speciation of organic fractions does matter for aerosol source apportionment. Part 3: combining off-line and online measurements. Sci. Total Environ. 690, 944–955. https://doi.org/10.1016/j.scitotenv.2019.06.378.
Sullivan, R.C., Guazzotti, S.A., Sodeman, D.A., Prather, K.A., 2007. Direct observations of the atmospheric processing of Asian mineral dust. Atmos. Chem. Phys. 7, 1213–1236. https://doi.org/10.5194/acp-7-1213-2007.
Thorpe, A., Harrison, R.M., 2008. Sources and properties of non-exhaust particulate matter from road traffic: a review. Sci. Total Environ. 400, 270–282. https://doi.org/10.1016/j.scitotenv.2008.06.007.
Tissari, J., Lyyränen, J., Hytönen, K., Sippula, O., Tapper, U., Frey, A., Saarnio, K., Pennanen, A.S., Hillamo, R., Salonen, R.O., Hirvonen, M.-R., Jokiniemi, J., 2008. Fine particle and gaseous emissions from normal and smouldering wood combustion in a conventional masonry heater. Atmos. Environ. 34, 7862–7873.
Tiwari, S., Tunved, P., Hopke, P.K., Srivastava, A.K., Bisht, D.S., Pandey, A.K., 2016. Observations of ambient trace gas and PM10 concentrations at Patna, Central Ganga Basin during 2013-2014: the influence of meteorological variables on atmospheric pollutants. Atmos. Res. 180, 138–149. https://doi.org/10.1016/j.atmosres.2016.05.017.
Tositti, L., Brattich, E., Masiol, M., Baldacci, D., Ceccato, D., Parmeggiani, S., Stracquadanio, M., Zappoli, S., 2014. Source apportionment of particulate matter in a large city of southeastern Po Valley (Bologna, Italy). Environ. Sci. Pollut. Res. 21, 872–890. https://doi.org/10.1007/s11356-013-1911-7.
Valotto, G., Squizzato, S., Masiol, M., Zannoni, D., Visin, F., Rampazzo, G., 2014. Elemental characterization, sources and wind dependence of PM1 near Venice, Italy. Atmos. Res. 143, 371–379. https://doi.org/10.1016/j.atmosres.2014.03.007.
Vecchi, R., Marcazzan, G., Valli, G., Ceriani, M., Antoniazzi, C., 2004. The role of atmospheric dispersion in the seasonal variation of PM1 and PM2.5 concentration and composition in the urban area of Milan (Italy). Atmos. Environ. 38, 4437–4446. https://doi.org/10.1016/j.atmosenv.2004.05.029.
Vecchi, R., Chiari, M., D'Alessandro, A., Fermo, P., Lucarelli, F., Mazzei, F., Nava, S., Piazzalunga, A., Prati, P., Silvani, F., Valli, G., 2008. A mass closure and PMF source apportionment study on the sub-micron sized aerosol fraction at urban sites in Italy. Atmos. Environ. 42, 2240–2253. https://doi.org/10.1016/j.atmosenv.2007.11.039.
Vecchi, R., Bernardoni, V., Fermo, P., Lucarelli, F., Mazzei, F., Nava, S., Prati, P., Piazzalunga, A., Valli, G., 2009. 4-hours resolution data to study PM10 in a "hot spot" area in Europe. Environ. Monit. Assess. 154, 283–300. https://doi.org/10.1007/s10661-008-0396-1.
Vecchi, R., Bernardoni, V., Valentini, S., Piazzalunga, A., Fermo, P., Valli, G., 2018. Assessment of light extinction at a European polluted urban area during wintertime: impact of PM1 composition and sources. Environ. Pollut. 233, 679–689. https://doi.org/10.1016/j.envpol.2017.10.059.
Vecchi, R., Piziali, F.A., Valli, G., Favaron, M., Bernardoni, V., 2019. Radon-based estimates of equivalent mixing layer heights: a long-term assessment. Atmos. Environ. 197, 150–158. https://doi.org/10.1016/j.atmosenv.2018.10.020.
Venturini, E., Vassura, I., Raffo, S., Ferroni, L., Bernardi, E., Passarini, F., 2014. Source apportionment and location by selective wind sampling and Positive Matrix Factorization. Environ. Sci. Pollut. Res. 21, 11634–11648. https://doi.org/10.1007/s11356-014-2507-6.
Viana, M., Kuhlbusch, T.A.J., Querol, X., Alastuey, A., Harrison, R.M., Hopke, P.K., Winiwarter, W., Vallius, M., Szidat, S., Prévôt, A.S.H., Hueglin, C., Bloemen, H., Wåhlin, P., Vecchi, R., Miranda, A.I., Kasper-Giebl, A., Maenhaut, W., Hitzenberger, R., 2008. Source apportionment of particulate matter in Europe: a review of methods and results. J. Aerosol Sci. 39, 827–849. https://doi.org/10.1016/j.jaerosci.2008.05.007.
Vincenti, B., Paris, E., Carnevale, M., Palma, A., Guerriero, E., Borello, D., Paolini, V., Gallucci, F., 2022. Saccharides as particulate matter tracers of biomass burning: a review. Int. J. Environ. Res. Publ. Health 19. https://doi.org/10.3390/ijerph19074387.
Vogel, A., Elbern, H., 2021. Identifying forecast uncertainties for biogenic gases in the Po Valley related to model configuration in EURAD-IM during PEGASOS 2012. Atmos. Chem. Phys. 21, 4039–4057. https://doi.org/10.5194/acp-21-4039-2021.
WHO, 2021. WHO Global Air Quality Guidelines. Particulate Matter (PM2.5 and PM10), Ozone, Nitrogen Dioxide, Sulfur Dioxide and Carbon Monoxide. World Health Organisation.
Yao, W., Zhao, Y., Chen, R., Wang, M., Song, W., Yu, D., 2023. Emissions of toxic substances from biomass burning: a review of methods and technical influencing factors. Processes 11, 853. https://doi.org/10.3390/pr11030853.
Zhou, L., Hopke, P.K., Paatero, P., Ondov, J.M., Pancras, J.P., Pekney, N.J., Davidson, C. I., 2004. Advanced factor analysis for multiple time resolution aerosol composition data. Atmos. Environ. 38, 4909–4920. https://doi.org/10.1016/j.atmosenv.2004.05.040.